

Chern Fermi-pockets and chiral topological pair density waves in kagomé superconductors

Sen Zhou^{1,2} and Ziqiang Wang³

¹CAS Key Laboratory of Theoretical Physics, Institute of Theoretical Physics, Chinese Academy of Sciences, Beijing 100190, China

²School of Physical Sciences & CAS Center for Excellence in Topological Quantum Computation, University of Chinese Academy of Sciences, Beijing 100049, China

³Department of Physics, Boston College, Chestnut Hill, MA 02467, USA

(Dated: October 14, 2021)

The recent discovery of novel charge density wave (CDW) [1, 2] and pair density wave (PDW) [3] in vanadium-based superconductors AV_3Sb_5 ($A = K, Rb, Cs$) [4] hints at new correlated and topological quantum states of itinerant electrons on the kagomé lattice. Here, we study the simplest kagomé lattice model and demonstrate the emergence of Chern Fermi surface pockets from the lightly doped orbital Chern insulator in the $2a_0 \times 2a_0$ complex CDW state near van Hove filling. The Chern Fermi pockets, of sizes comparable to those detected by quantum oscillations, carry large Berry curvature, orbital magnetic moment, and a Hall conductivity as in the observed intrinsic anomalous Hall effect. More intriguingly, the elliptical Chern Fermi pockets, connected by $\frac{3}{4}Q_{\text{Bragg}}$ in the 3Q directions, are shown to produce novel $\frac{4}{3}a_0 \times \frac{4}{3}a_0$ PDWs as observed in the superconducting and pseudogap phases of CsV_3Sb_5 [3]. We find that the incipient PDW is a never-before-encountered chiral topological PDW superconductor. It is protected by an intertwined secondary uniform superconducting condensate due to the hexagonal symmetry and hosts chiral Majorana edge modes. Our findings reveal a new orbital-based mechanism and a prominent kagomé materials platform for *intrinsic* chiral topological density waves and superconductors.

I. INTRODUCTION

The field of transition-metal kagomé lattice materials has leapt forward with the recent discovery of superconductivity in a new family of vanadium-based kagomé metals AV_3Sb_5 ($A = K, Rb, Cs$) [4, 5]. In contrast to the insulating kagomé compounds extensively studied for quantum spin liquids and doped Mott insulators [6–8], AV_3Sb_5 are nonmagnetic correlated metals with itinerant electrons traversing the unique kagomé lattice structure that geometrically frustrates kinetic motion due to quantum interference. They are complementary to the (Fe, Co, Mn)-based itinerant kagomé magnets that exhibit correlated topological phenomena such as massive spin-polarized Dirac fermions [9, 10], magnetic Weyl semimetals [11–13], Berry curvature induced orbital magnetism [14], but have remained nonsuperconducting at low temperatures.

All AV_3Sb_5 undergo charge density wave (CDW) transitions below $T_{\text{cdw}} \sim 78 - 103$ K and superconducting (SC) transitions below $T_c \sim 0.9 - 2.5$ K to become rare kagomé lattice superconductors. Both the diagonal and the off-diagonal long-range ordered states turn out to be highly intriguing and unconventional. While charge order has been confirmed to be a $2a_0 \times 2a_0$ 3Q-CDW in the kagomé plane stacked along the c -axis [1–3, 15–18], it surprisingly produces giant anomalous Hall effect (AHE) despite the absence of magnetism [19, 20]. Scanning tunneling microscopy (STM) imaging of KV_3Sb_5 observed that the CDW responds to an applied magnetic field differently when the field direction is reversed along the c -axis [1], suggesting spontaneously time-reversal symmetry (TRS) breaking. Although the robustness of the STM observation is controversial [21, 22], evidence for TRS breaking has been detected in μ SR experiments [23, 24]. At low temperatures, STM experiments in CsV_3Sb_5 reveal the coexistence of strong-coupling superconductivity with $2a_0 \times 2a_0$ CDW and $4a_0$ unidirectional charge order [2, 3]. Remarkably, a 3Q pair density wave (PDW) with $\frac{4}{3}a_0 \times \frac{4}{3}a_0$ period was discovered

that spatially modulates the SC gap and coherence peaks [3]. Moreover, the phenomenology of the PDW is striking compared to that in high- T_c cuprates: it is detectable in the vortex core and above H_{c2} , emerges as a “mother state” above T_c , and is responsible for the observed pseudogap behavior. Here, we demonstrate theoretically that the essential part of these highly unusual properties is captured by a doped orbital Chern insulator on the kagomé lattice, and the emergent Chern Fermi surface pockets provide a new mechanism for orbital-driven intrinsic chiral topological superconductivity.

II. MODEL AND UNIFORM STATE

In the AV_3Sb_5 compounds, V atoms form an ideal kagomé lattice coordinated by Sb atoms, while the alkali atoms (A) intercalate between the kagomé layers. They have very similar band structures predicted by the density functional theory (DFT) [5, 16]. There is an electron-like Fermi surface (FS) around the center of the hexagonal Brillouin zone (BZ) derived from the Sb p_z orbital, while the actions of the low-energy vanadium d -orbitals are located around the zone boundary, forming quasi-2D FS sheets close to the van Hove (vH) singularities. The band dispersions measured by angle-resolved photoemission spectroscopy (ARPES) show overall agreement with the DFT predications [4, 25–29].

To capture the most essential physics of a d band crossing the Fermi level near the vH point, we consider the one-orbital model on the kagomé lattice as depicted in Fig. 1a with the lattice constant $a_0 \equiv 1$. The two basis vectors are $\mathbf{a}_1 = (1, 0)$ and $\mathbf{a}_2 = (-\frac{1}{2}, \frac{\sqrt{3}}{2})$ and the reciprocal lattice vectors $\mathbf{G}_1 = (0, \frac{4\pi}{\sqrt{3}})$ and $\mathbf{G}_2 = (-2\pi, -\frac{2\pi}{\sqrt{3}})$. This also defines the related third direction $\mathbf{a}_3 = -\mathbf{a}_1 - \mathbf{a}_2$ and $\mathbf{G}_3 = -\mathbf{G}_1 - \mathbf{G}_2$. The location of the *three* sublattices in a unit cell at \mathbf{r} is given by $\mathbf{r}_1 = \mathbf{r} - \frac{1}{2}\mathbf{a}_3$, $\mathbf{r}_2 = \mathbf{r}$, and $\mathbf{r}_3 = \mathbf{r} + \frac{1}{2}\mathbf{a}_1$. The kagomé lattice is

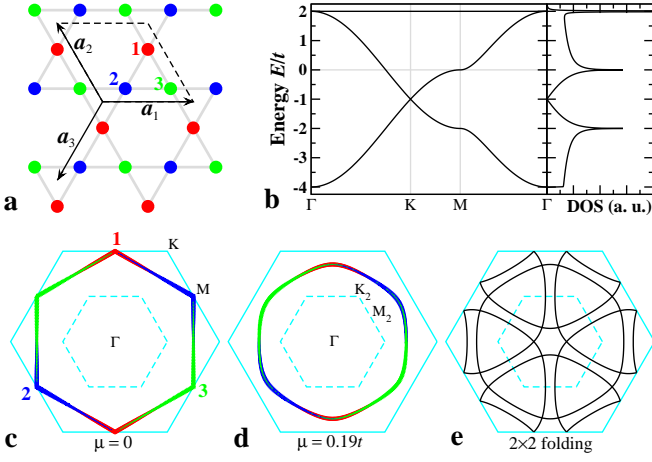


FIG. 1: **Itinerant fermions on kagomé lattice.** **a**, Lattice structure. The *three* sublattices are denoted by red (1), blue (2), and green (3) circles. $a_{1,2,3}$ are lattice vectors and $a_{1,2}$ defines the unit cell. **b**, Band dispersion and DOS. Fermi level at vH filling is marked by the grey line at $\mu = 0$. **c**, FS at vH filling in the hexagonal BZ (solid cyan curves). Thickness of colored lines and numbers display the sublattice contents. The high symmetry points $\Gamma = (0, 0)$, $K = (\pm \frac{4\pi}{3}, 0)$, $(\pm \frac{2\pi}{3}, \pm \frac{2\pi}{\sqrt{3}})$ and $M = (0, \pm \frac{2\pi}{\sqrt{3}})$, $(\pm \pi, \pm \frac{\pi}{\sqrt{3}})$. **d**, Sublattice resolved FS at $\mu = 0.19t$ for electron doping above vH filling. Dashed cyan curves enclose the 2×2 reduced BZ with the resulting high symmetry points denoted by $K_2 = \frac{1}{2}K$ and $M_2 = \frac{1}{2}M$. **e**, FS in **d** folded by the 2×2 BZ boundary.

composed of corner-sharing up and down triangles (Fig. 1a), and a generic tight-binding model with nearest-neighbor (nn) hopping can be written as,

$$H = - \sum_{(\alpha\beta\gamma)\mathbf{r}} \left[t_{\alpha\beta}^u(\mathbf{r}) c_{\alpha\mathbf{r}}^\dagger c_{\beta\mathbf{r}} + t_{\alpha\beta}^d(\mathbf{r}) c_{\alpha\mathbf{r}}^\dagger c_{\beta\mathbf{r}-\mathbf{a}_\gamma} + h.c. \right] - \mu n_{\alpha\mathbf{r}}, \quad (1)$$

where $c_{\alpha\mathbf{r}}^\dagger$ creates an electron on sublattice α in unit cell \mathbf{r} , $t_{\alpha\beta}^{u,d}(\mathbf{r})$ are the \mathbf{r} -dependent nn hoppings in the up and down triangles between sublattices α and β , μ is the chemical potential, and $n_{\alpha\mathbf{r}} = c_{\alpha\mathbf{r}}^\dagger c_{\alpha\mathbf{r}}$ is the density operator. The sublattice indices run over $(\alpha, \beta, \gamma) = (1, 2, 3), (2, 3, 1), (3, 1, 2)$ and spin indices are left implicit.

The model in Eq. (1) highlights the unique geometry of the kagomé lattice, which plays a crucial role in the charge ordered state to be discussed below. We rewrite

$$H = - \sum_{(\alpha\beta\gamma)\mathbf{r}} \left[t_{\alpha\beta}^+(\mathbf{r}) \chi_{\alpha\beta}^+(\mathbf{r}) + t_{\alpha\beta}^-(\mathbf{r}) \chi_{\alpha\beta}^-(\mathbf{r}) + h.c. \right] - \mu n_{\alpha\mathbf{r}}, \quad (2)$$

where $t_{\alpha\beta}^\pm = \frac{1}{2}(t_{\alpha\beta}^u \pm t_{\alpha\beta}^d)$ and the corresponding symmetric (+) and antisymmetric (−) nn bond operators,

$$\chi_{\alpha\beta}^\pm(\mathbf{r}) = c_{\alpha\mathbf{r}}^\dagger c_{\beta\mathbf{r}} \pm c_{\alpha\mathbf{r}}^\dagger c_{\beta\mathbf{r}-\mathbf{a}_\gamma}. \quad (3)$$

For a kagomé lattice with uniform nn hopping, $t_{\alpha\beta}^+(\mathbf{r}) = t$ and $t_{\alpha\beta}^-(\mathbf{r}) = 0$. The corresponding band dispersion and density of states (DOS) are shown in Fig. 1b. A uniform $t_{\alpha\beta}^-(\mathbf{r}) = \delta \neq 0$ produces an intra-cell breathing kagomé lattice [30] without breaking lattice translation symmetry. Electron correlations

can drive a bond ordered CDW and produce a spatially modulated hopping $t_{\alpha\beta}^\pm(\mathbf{r}) \neq 0$. In particular, a $t_{\alpha\beta}^-(\mathbf{r}) = \delta \cos(\mathbf{Q} \cdot \mathbf{r})$ leads to a translation symmetry breaking breathing kagomé lattice and a CDW with wave vector $\mathbf{Q} \neq \mathbf{G}$.

III. COMPLEX CDW AND CHERN FERMİ POCKETS

At a band filling $n_{\text{vH}} = 5/12$ or $\mu = 0$, the sublattice-resolved Fermi surface (FS) is the hexagon connecting the vH singularity at the M points of the BZ in Fig. 1c. Theoretical studies at this vH filling have demonstrated a rich set of instabilities toward correlated states due to the unique sublattice quantum interference effects [31–33]. When extended Coulomb interactions V play a more important role than the local Hubbard U , the leading instability is a $2a_0 \times 2a_0$ bond ordered CDW. It is remarkable that the single-orbital model prediction turns out to be consistent with the 3Q CDW observed at $\mathbf{Q}_{\text{cdw}}^\alpha = \frac{1}{2}\mathbf{G}_\alpha$ in the multi-orbital AV_3Sb_5 [1–3] and with first principle DFT calculations [16], signifying the essential physics can be captured by the proximity of the Fermi level to the d -bands vH singularities.

Motivated by the conjecture [1] of spontaneous TRS breaking circulating loop currents [34–36] possibly detected by STM experiments, several theoretical model studies explored 3Q CDWs with imaginary or complex bond order hosting link current and plaquette flux [37–40]. This state corresponds to complex expectation values of the antisymmetry bond operator in Eq. (3) and can be described by

$$H_{\text{cdw}} = \sum_{(\alpha\beta\gamma)\mathbf{r}} \rho_\gamma \cos(\mathbf{Q}_{\text{cdw}}^\gamma \cdot \mathbf{r}) \chi_{\alpha\beta}^-(\mathbf{r}) + h.c., \quad (4)$$

where the amplitude and phase ρ_γ is complex in general.

A crucial point to realize is that the actual Fermi level is above the vH point of the $d_{xz/yz}$ band at M in all three realistic AV_3Sb_5 compounds, as shown by DFT calculations [16] and ARPES measurements [25–29]. It is thus important to study the complex bond ordered phase described by Eq. (4) close to but not at vH filling, which, as we show below, results in a novel metallic 3Q CDW state and an emergent primary PDW state detected by STM in CsV_3Sb_5 recently [3].

We thus study the physics above vH filling ($n \gtrsim n_{\text{vH}}$) by setting the symmetric hopping $t_{\alpha\beta}^+(\mathbf{r}) = t$ uniform as the energy unit and the chemical potential $\mu = 0.19t$ in Eq. (2). Fig. 1d shows the sublattice resolved FS which describes well the FS contours for the $d_{xz/yz}$ band in DFT [16] at both $k_z = 0$ and $k_z = \pi$. The 3Q CDW described by H_{cdw} amounts to a correlation-induced breathing modulation of the antisymmetric hopping $t_{\alpha\beta}^-(\mathbf{r}) = \rho_\gamma \cos(\mathbf{Q}_{\text{cdw}}^\gamma \cdot \mathbf{r})$ in Eq. (2). Diagonalizing H for equal amplitudes in the 3Q directions $\rho = (0.1 + 0.3i)(1, 1, 1)$, we obtain the $2a_0 \times 2a_0$ complex CDW state shown in Fig. 2.

The modulation of the antisymmetric $\chi_{\alpha\beta}^-(\mathbf{r})$ leads to three different current-carrying bonds and the Star of David pattern in Fig. 2a. Accumulating the link phases around the plaquette produces four gauge-independent plaquette fluxes $\phi_{1,\dots,4}$ in the shaded 2×2 unit cell. Although the flux is staggered and the total flux $\Phi = \phi_1 + 3\phi_2 + 2\phi_3 + 6\phi_4$ is zero by symmetry, the

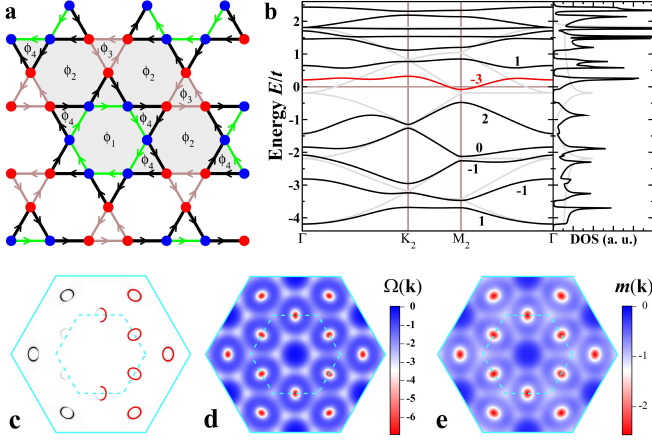


FIG. 2: **Complex CDW and Chern Fermi pockets.** **a**, Schematics of the $2a_0 \times 2a_0$ CDW state. Electron density is 0.878 (0.810) on the red (blue) sites. Three complex hoppings on the black, green, and grey bonds are $0.499 \pm 0.123i$, $0.345 \pm 0.162i$, and $0.349 \pm 0.110i$, respectively, giving rise to four independent plaquette fluxes $\phi_{1,\dots,4} = (0.840, -0.028, -0.291, 0.014)\pi$. The net flux through the unit cell (shaded grey) is zero. **b**, Band dispersion in the folded BZ and DOS. Bands are marked by corresponding Chern numbers. **c**, Intensity plot of the DOS at the Fermi level, showing the spectral weight of the CFPs. Locations of the pockets are superimposed as red solid ellipses on the right half of the BZ. **d**, Berry curvature distribution $\Omega(\mathbf{k})$ of the $C=-3$ Chern band (red) in **b**. **e**, Orbital magnetic moment distribution $m(\mathbf{k})$ of the $C=-3$ Chern band in unit of $ta_0^2 e/2\hbar$.

complex CDW breaks TRS but maintains inversion symmetry, and gives rise to topological Chern bands on the kagomé lattice. The band dispersions, marked by the corresponding Chern numbers C , and the DOS are shown in Fig. 2b in the reduced zone. The Fermi level crosses the red Chern band with $C=-3$ near the M_2 points, which amounts to electron doping of a Chern insulator at vH filling. Since the nontrivial Chern numbers are induced by the TRS-breaking orbital currents, the CDW metal is a doped orbital Chern insulator with the emergent elliptical Chern Fermi pockets (CFPs) shown in Fig. 2c. Residing along Γ -K and Γ - M_2 directions due to the 2×2 FS folding (Fig. 1e), each FS pocket occupies a volume of $\sim 0.56\%$ of the original BZ (Fig. 2c). We note that FS pockets of a similar size have been detected recently by quantum oscillations [41, 42], although the multiorbital nature of the V d -bands prevents a more detailed comparison.

To reveal the riveting properties of the CFPs inherited from the topological orbital Chern insulator, we calculate the Berry curvature and orbital magnetic moment (See Methods) of the hosting $C=-3$ Chern band. Fig. 2d shows that the Berry curvature in momentum space $\Omega(\mathbf{k})$ concentrates heavily on the CFPs. This leads to a large contribution to the 2D anomalous Hall conductivity beyond that from fully occupied Chern bands in Fig. 2b, $\sigma_{xy} = -2\frac{e^2}{h} - 2\frac{e^2}{h} \int_0^{\frac{d^2k}{2\pi}} \Omega(\mathbf{k}) \simeq -1.1\frac{e^2}{h}$. Using the c -axis lattice constant $c \simeq 8.95\text{\AA}$ [5], we have $\sigma_{xy}/c \simeq 474\Omega^{-1}\text{cm}^{-1}$ in magnitude, which semi-quantitatively accounts for the observed large *intrinsic* AHE ($\sim 500\Omega^{-1}\text{cm}^{-1}$) [19, 20]. The orbital magnetic moment $m(\mathbf{k})$ is plotted in Fig. 2e in unit of $ta_0^2 e/2\hbar \simeq 1.91\mu_B$ for $a_0 \simeq 5.4\text{\AA}$

and $t = 0.5\text{eV}$, i.e. a 3eV bandwidth of the $d_{xz/yz}$ -band [5, 16]. The orbital moment, as large as $\sim -5\mu_B$, concentrates on the CFPs and couples to an applied magnetic field along the c -axis via the orbital Zeeman effect $-m(\mathbf{k})B_z$, which can result in strong \mathbf{k} -dependent band renormalizations. Moreover, the *intrinsic* thermodynamic orbital magnetization is calculated (Methods) to be $M \simeq 0.078\mu_B$ per V, large enough to be detectable by thermodynamic measurements.

IV. CHIRAL TOPOLOGICAL PDW

The dynamically generated FS pockets are connected by well-defined momenta due to the band-folding. Fig 3a displays the 12 color coded CFPs. Pockets of the same color are related by the reciprocal lattice vectors of the $2a_0 \times 2a_0$ CDW $\mathbf{G}_{2a_0} = \frac{1}{2}\mathbf{G}$. Those of different colors are, in contrast, connected by *new* wave vectors $\mathbf{Q}_{4a_0} = \frac{1}{4}\mathbf{G}$ and $\mathbf{Q}_{\frac{4}{3}a_0} = \frac{3}{4}\mathbf{G}$ in all 3Q directions, enabling new correlated quantum states that can coexist with the $2a_0 \times 2a_0$ CDW.

Note that neither \mathbf{Q}_{4a_0} nor $\mathbf{Q}_{\frac{4}{3}a_0}$ leads to full nesting because of the ellipticity of the pockets (Fig. 3b). Moreover, since the pockets are all electron-like, additional 3Q CDWs at these wave vectors cannot gap out the pockets, but reshape them to different sizes around Γ in the 4×4 reduced BZ (see Methods). This phase has not appeared experimentally, possibly because it is ineffective at lowering energy. A Ginzburg-Landau analysis [43] indicates a unidirectional 1Q CDW with $4a_0$ periodicity is also possible, which breaks both translation and rotation symmetry. A striped $4a_0$ charge order was indeed observed by STM on the Sb surface in CsV_3Sb_5 [2, 3].

The path toward a stable correlated ground state can arise in the particle-particle channel through the formation of a PDW with wave vector \mathbf{Q}_{pdw} . A PDW pairs a spin-down electron at momentum \mathbf{k} with a spin-up electron at $-\mathbf{k} + \mathbf{Q}_{\text{pdw}}$. In contrast to a CDW, it does not require the connected CFPs to be electron and hole like to produce a large susceptibility. As shown in Fig. 3a, the outer CFPs carry the majority of the spectral weight (Fig. 2c) and can be more susceptible to a stabilizing 3Q PDW with $\frac{4}{3}a_0 \times \frac{4}{3}a_0$ periodicity. The energetically favorable 3Q PDW wave vector is therefore $\mathbf{Q}_{\text{pdw}} = \mathbf{Q}_{\frac{4}{3}a_0}$, which connects each of the six outer elliptical pockets in Fig. 3a with its two neighbors.

We next study the properties of the 3Q PDW in connection to the experimental observation of the $\frac{4}{3}a_0 \times \frac{4}{3}a_0$ PDW that emerges as a pseudogap state above T_c and coexists with superconductivity below T_c in CsV_3Sb_5 [3]. In view of the relatively weak local Coulomb repulsion in AV_3Sb_5 , we consider the simplest onsite, spin-singlet pairing,

$$H_{\text{pdw}} = - \sum_{\alpha\mathbf{r}} 2\Delta_{\text{pdw}}^\alpha(\mathbf{r}) c_{\alpha\downarrow}^\dagger(\mathbf{r}) c_{\alpha\uparrow}^\dagger(\mathbf{r}) + h.c., \quad (5)$$

where $\Delta_{\text{pdw}}^\alpha(\mathbf{r})$ is the 3Q PDW order parameter. It is a coherent superposition of six PDWs with wavevectors $\pm\mathbf{Q}_{\text{pdw}}^{1,2,3}$,

$$\Delta_{\pm\mathbf{Q}_{\text{pdw}}}^\alpha(\mathbf{r}) = \Delta_p^\alpha e^{\pm i\mathbf{Q}_{\text{pdw}}^\alpha \cdot (\mathbf{r}-\mathbf{r}_0)}, \quad (6)$$

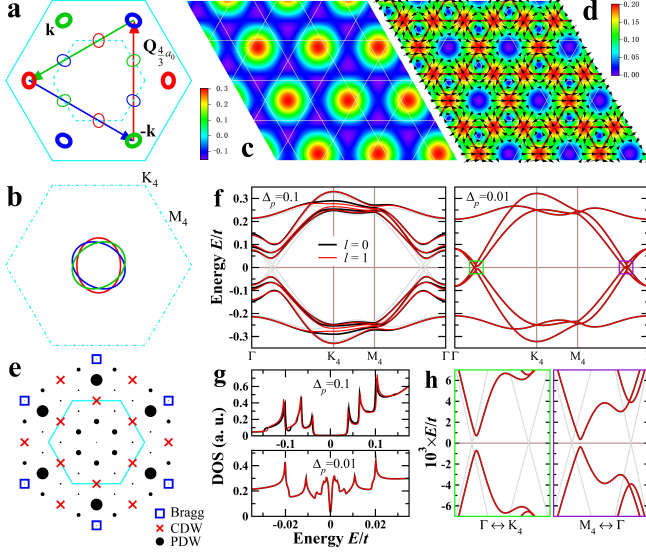


FIG. 3: **3Q PDW and gapped Chern Fermi pockets.** **a**, Structure diagram of the CFPs. Pockets drawn in thick colored lines are connected by wave vectors $\mathbf{Q}_{\frac{4}{3}a_0}$ and carry most of the spectral weight (Fig. 2c). **b**, Folded elliptical pockets in the 4×4 reduced BZ. **c**, Spatial distribution of the $\frac{4}{3}a_0 \times \frac{4}{3}a_0$ real PDW₀ order parameter for $\Delta_p = 0.1t$, showing a triangular lattice in the background kagomé lattice (white lines). **d**, Spatial distribution of the $\frac{4}{3}a_0 \times \frac{4}{3}a_0$ complex PDW₁ order parameter for $\Delta_p = 0.1t$, with amplitude represented by color intensity and phase denoted by arrows. The emergent vortex-antivortex kagomé lattice is shown by red lines with vortex cores located at the center of triangles and hexagons. **e**, Fourier peaks under coexisting $2a_0 \times 2a_0$ CDW and $\frac{4}{3}a_0 \times \frac{4}{3}a_0$ PDW_{0,1}. **f**, Low-energy BdG quasiparticle bands in the 4×4 folded BZ in **b**. Grey lines correspond to $\Delta_p = 0$. **g**, Low-energy DOS of PDW_{0,1}. Top panel ($\Delta_p = 0.1t$) shows three pairs of coherence peaks at the PDW gaps of the three low-energy bands. Lower panel ($\Delta_p = 0.01t$) shows a V-shaped SC gap. A $k_B T = 10^{-4}t$ thermal broadening is applied. **h**, Zoom-in of low-energy band dispersions inside green and violet boxes in the right panel of **f**, showing a full gap due to PDW_{0,1} induced uniform superconductivity.

where $\Delta_p^\alpha = \Delta_p e^{i\phi_\alpha}$ is the PDW amplitude and phase factor, and \mathbf{r}_0 is at the C_6 /inversion center of the CDW in Fig. 2a. We find that the most prominent 3Q PDW in the Landau-Ginzburg theory on the hexagonal lattice [44] can be written as

$$\Delta_{\text{pdw}}^\alpha(\mathbf{r}) = \Delta_p \sum_{\beta} e^{i\phi_\beta} \cos[\mathbf{Q}_{\text{pdw}}^\beta \cdot (\mathbf{r}_\alpha - \mathbf{r}_0)], \quad (7)$$

where the relative sublattice phase $\phi_\beta = \ell(\beta - 1)2\pi/3$ with integer ℓ . The spatial distribution of the order parameter shows that $\ell = 0$ describes a real PDW₀ forming a $\frac{4}{3}a_0 \times \frac{4}{3}a_0$ triangle lattice (Fig. 3c). Intriguingly, for $\ell = 1$, a complex PDW₁ emerges in a $\frac{4}{3}a_0 \times \frac{4}{3}a_0$ vortex-antivortex kagomé lattice (Fig. 3d), with the zeros of the order parameter located at the center of hexagons and triangles. The latter is the conjectured roton-PDW [3], and a roton corresponds to a tightly bound vortex-antivortex pair.

Including H_{pdw} , the total Hamiltonian can be diagonalized by solving the Bogoliubov-de Gennes (BdG) equations. The

Fourier peaks of the resulting charge and pair densities are plotted in Fig. 3e. The corresponding quasiparticle bands are shown in Fig. 3f in the 4×4 folded BZ for PDW_{0,1}. The CFPs of complex CDW state are fully gapped by $\frac{4}{3}a_0 \times \frac{4}{3}a_0$ PDW_{0,1} with amplitude $\Delta_p = 0.1t$ in the left panel in Fig. 3f. Specifically, three gapped quasiparticle bands, stemming from the three-colored CFPs that complete the C_6 rotational symmetry, emerge with minimum gap loci offset from the respective Fermi momentum (Fig. 3f). Remarkably, the low-energy DOS in Fig. 3g (top panel) reveals a particle-hole symmetric gap and three pairs of PDW peaks, consistent with the DOS spectrum observed by STM on CsV₃Sb₅ in the SC state [3].

A primary PDW is known to induce subsidiary electronic density wave orders in the Landau-Ginzburg theory [44–47]. Intriguingly, due to the unique hexagonal symmetry, $\sum_{\alpha} \mathbf{Q}_{\text{pdw}}^\alpha = 0$ and a secondary uniform SC order [44] emerges unexpectedly and has the form

$$\Delta_0^{(\alpha,\beta,\gamma)} \propto \Delta_{\mathbf{Q}_{\text{pdw}}^\alpha}(\mathbf{r}) \Delta_{\mathbf{Q}_{\text{pdw}}^\beta}(\mathbf{r}) \Delta_{\mathbf{Q}_{\text{pdw}}^\gamma}^*(\mathbf{r}) = \Delta_p^3 \phi^\alpha \phi^\beta \phi^{\gamma*}. \quad (8)$$

Accordingly, a uniform s -wave SC with $\Delta_0 \sim \Delta_p^3$ or a uniform $p_x + ip_y$ SC with $\Delta_0^{(1,2,3)} \sim \Delta_p^3(1, e^{2\pi i/3}, e^{4\pi i/3})$ coexists with the real PDW₀ or the complex PDW₁, respectively. The induced uniform condensate ensures that the 3Q PDW possesses an intertwined BCS instability and the CFPs are gapped by arbitrarily small Δ_p . Fig. 3f (right panel) shows the quasiparticle dispersion of PDW_{0,1} for a much smaller $\Delta_p = 0.01t$, which upon zooming in, still exhibits a full gap in Fig. 3h. The low energy DOS (Fig. 3g, bottom panel) shows a V-shaped SC gap inside the PDW pseudogap at very low temperatures, located approximately at 0.7meV and 10meV respectively for $t = 0.5\text{eV}$, in line with STM observations [3]. The subsidiary density waves and uniform superconductivity can remain long-range ordered even when the same for the primary PDW is suppressed by quantum and thermal phase fluctuations [45, 48].

Strikingly, the incipient PDW with fully gapped CFPs carries an integer topological invariant $\mathcal{N} \in \mathbb{Z}$ in 2D, since the BdG Hamiltonian is in class D [49]. When the occupied BdG quasiparticle bands in Fig. 3e hold a total Chern number \mathcal{N} , there will be \mathcal{N} number of charge neutral chiral Majorana edge modes (CMEMs) at the sample boundary. Calculating the total Chern number, we obtain $\mathcal{N} = 2$ for both PDW_{0,1}. Under inversion symmetric open boundaries in the y -direction (Fig. 4a), we calculate and plot in Fig. 4b–c the spectrum of the BdG Hamiltonian for PDW_{0,1}, respectively, as a function of the momentum k_x in the periodic x -direction. Both states exhibit two CMEMs of equal chirality inside the PDW gap (red and blue) that pairwise localize on the opposite edges (Fig. 4d). For comparison, the spectrum of a uniform s -wave SC in the complex CDW phase in the absence of the PDW reveals two similar CMEMs in Fig. 4e, which can be understood as a chiral topological SC achieved by s -wave pairing in a doped orbital Chern insulator. We thus conclude that the 3Q real and complex PDWs are unprecedented chiral topological PDW superconductors with $\mathcal{N} = 2$, hosting CMEMs and vortex Majorana zero modes protected by the intrinsic topological gap of the CFPs. Zero-bias conductance peaks in vortex cores have indeed been detected by STM on CsV₃Sb₅ [15].

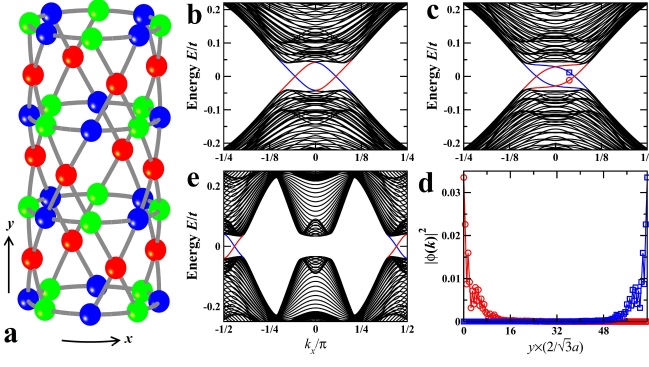


FIG. 4: **Chiral topological PDW and Majorana edge modes.** **a**, Schematics of a cylindrical kagomé lattice with open boundaries in y -direction. A single 4×4 supercell is shown. Systems studied contain $L_x \times L_y$ supercells and an infinite L_x is used along the periodic direction in calculations. **b**, Low-energy quasiparticle spectrum of the real PDW_0 at $\Delta_p = 0.1t$, showing two in-gap CMEMs (blue and red). $L_y = 64$ with 4×4 supercell. **c**, Same as in **b**, but for the complex 3Q PDW_1 . **d**, Distribution along y -direction of the supercell averaged wavefunction amplitudes corresponding to the two in-gap CMEMs indicated in **c** at $k_x = 3\pi/80$ (red circle and blue square), showing localization at the opposite edges illustrated in **a**. **e**, Low-energy quasiparticle spectrum of a uniform s -wave superconductor with $\Delta_s = 0.03t$ coexisting with the complex CDW. $L_y = 96$ with 2×2 supercell.

V. DISCUSSION

The microscopic origin of the pairing interaction in the multiorbital AV_3Sb_5 is beyond the scope of this work. The observed primary 3Q PDW in the pseudogap and SC phases in CsV_3Sb_5 [3] suggests that electronic fluctuations in the complex CDW phase, including from orbital current or flux density [50–52], can mediate pairing interactions with substantial

momentum space anisotropy to generate the 3Q PDW from the CFPs. An independent uniform s -wave pairing may also be present in real materials, in view of the electron-phonon coupling. Depending on the relative phases, adding an independent uniform s -wave condensate Δ_s can produce gap closing and reopening transitions for both the real and complex 3Q PDWs (see Methods). Interestingly, due to the nonzero angular momentum of the complex PDW_1 and its subsidiary $p_x + ip_y$ condensate, the independent Δ_s leads to C_6 rotation symmetry breaking down to C_2 in the coexisting SC state.

Our findings reveal that doped orbital Chern insulators with CFPs embody a rich set of correlated and topological states including chiral topological PDW superconductors. They can emerge from itinerant electrons on the kagomé lattice lightly doped away from the νH filling, and capture an essential part of the unconventional phenomenology in AV_3Sb_5 superconductors. The PDW mechanism for intrinsic chiral topological superconductivity and other novel paired states via doped orbital Chern insulators is potentially relevant for twisted bilayer graphene and other hexagonal quantum materials.

We thank Binghai Yan, Kun Jiang, Jiangping Hu, Jiaxin Yin, Zahid Hasan, He Zhao, Ilija Zeljkovic, Hu Miao, Stephen Wilson, and especially Hui Chen and Hongjun Gao for valuable discussions. S. Z. is supported by the Strategic Priority Research Program of CAS (Grant No. XDB28000000) and the National Natural Science Foundation of China (Grants No. 11974362 and No. 12047503). Z. W. is supported by the U.S. Department of Energy, Basic Energy Sciences (Grant No. DE-FG02-99ER45747) and by the Cottrell SEED Award No 27856 from Research Corporation for Science Advancement. Numerical calculations were performed on the HPC Cluster of ITP-CAS. Z. W. thanks Aspen Center for Physics for hospitality and acknowledges the support of NSF Grant No. PHY-1066293.

-
- [1] Y.-X. Jiang, et al., Unconventional chiral charge order in kagome superconductor KV_3Sb_5 , *Nat. Mater.* **20**, 1353 (2021).
 - [2] H. Zhao, et al., Cascade of correlated electron states in a kagome superconductor CsV_3Sb_5 , arXiv:2103.03118, *Nature* (2021). <https://doi.org/10.1038/s41586-021-03946-w>.
 - [3] H. Chen, et al., Roton pair density wave in a strong-coupling kagome superconductor, arXiv:2103.09188, *Nature* (2021). <https://doi.org/10.1038/s41586-021-03983-5>.
 - [4] B. R. Ortiz, et al., CsV_3Sb_5 : A Z_2 topological kagome metal with a superconducting ground state, *Phys. Rev. Lett.* **125**, 247002 (2020).
 - [5] B. R. Ortiz, et al., New kagome prototype materials: discovery of KV_3Sb_5 , RbV_3Sb_5 , and CsV_3Sb_5 , *Phys. Rev. Mater.* **3** (2019).
 - [6] T.-H. Han, J. S. Helton, S. Chu, D. G. Nocera, J. A. Rodriguez-Rivera, C. Broholm, and Y. S. Lee, Fractionalized excitations in the spin-liquid state of a kagome lattice antiferromagnet, *Nature* **492**, 406 (2012).
 - [7] M.R. Norman, Herbertsmithite and the search for the quantum spin liquid, *Rev. Mod. Phys.* **88**, 041002 (2016).
 - [8] W.-H. Ko, P. A. Lee, and X.-G. Wen, Doped kagome system as exotic superconductor, *Phys. Rev. B* **79**, 214502 (2009).
 - [9] L. Ye, et al., Massive Dirac fermions in a ferromagnetic kagome metal, *Nature* **555**, 638 (2018).
 - [10] J.-X. Yin, et al., Giant and anisotropic many-body spin-orbit tunability in a strongly correlated kagome magnet, *Nature* **562**, 91 (2018).
 - [11] N. Morali, et al., Fermi-arc diversity on surface terminations of the magnetic Weyl semimetal $\text{Co}_3\text{Sn}_2\text{S}_2$, *Science* **365**, 1286 (2019).
 - [12] D. F. Liu, et al., Magnetic Weyl semimetal phase in a kagomé crystal, *Science* **365**, 1282 (2019).
 - [13] E. Liu, et al., Giant anomalous Hall effect in a ferromagnetic kagome-lattice semimetal, *Nat. Phys.* **14**, 1125 (2018).
 - [14] J.-X. Yin, Negative flat band magnetism in a spin-orbit-coupled correlated kagome magnet, *Nat. Phys.* **15**, 443 (2019).
 - [15] Z. Liang, et al., Three-dimensional charge density wave and surface-dependent vortex-core states in a kagome superconductor CsV_3Sb_5 , *Phys. Rev. X* **11**, 031026 (2021).
 - [16] H. Tan, Y. Liu, Z. Wang, and B. Yan, Charge density waves and electronic properties of superconducting kagome metals, *Phys. Rev. Lett.* **127**, 046401 (2021).

- [17] H. Li, et al., Observation of unconventional charge density wave without acoustic phonon anomaly in kagome superconductors AV_3Sb_5 ($A=Rb, Cs$), *Phys. Rev. X* **11**, 031050 (2021).
- [18] B. R. Ortiz, et al., Fermi surface mapping and the nature of charge density wave order in the kagome superconductor CsV_3Sb_5 , arXiv:2104.07230, to be published in *Phys. Rev. X* (2021).
- [19] S.-Y. Yang, et al., Giant, unconventional anomalous Hall effect in the metallic frustrated magnet candidate, KV_3Sb_5 , *Sci. Adv.* **6**, eabb6003 (2020).
- [20] F. H. Yu, T. Wu, Z. Y. Wang, B. Lei, W. Z. Zhuo, J. J. Ying, and X. H. Chen, Concurrence of anomalous Hall effect and charge density wave in a superconducting topological kagome metal, *Phys. Rev. B* **104** L041103 (2021).
- [21] H. Li, et al., Rotation symmetry breaking in the normal state of a kagome superconductor KV_3Sb_5 , arXiv:2104.08209 (2021)
- [22] H. Li, et al., No indication of chiral flux current in the topological kagome metal CsV_3Sb_5 , arXiv:2107.11326 (2021)
- [23] C. Mielke III, et al., Time-reversal symmetry-breaking charge order in a correlated kagome superconductor, arXiv:2106.13443 (2021).
- [24] L. Yu, et al., Evidence of a hidden flux phase in the topological kagome metal CsV_3Sb_5 , arXiv:2107.10714 (2021).
- [25] Z. Wang, et al., Distinctive momentum dependent charge-density-wave gap observed in CsV_3Sb_5 superconductor with topological Kagome lattice, arXiv:2104.05556 (2021).
- [26] K. Nakayama, Y. Li, M. Liu, Z. Wang, T. Takahashi, Y. Yao, and T. Sato, Multiple energy scales and anisotropic energy gap in the charge-density-wave phase of kagome superconductor CsV_3Sb_5 , arXiv:2104.08042 (2021).
- [27] Y. Hu, et al., Charge-order-assisted topological surface states and flat bands in the kagome superconductor CsV_3Sb_5 , arXiv:2104.12725 (2021).
- [28] M. Kang, et al., Twofold van Hove singularity and origin of charge order in topological kagome superconductor CsV_3Sb_5 , arXiv:2105.01689 (2021).
- [29] H. Luo, et al., Electronic nature of charge density wave and electron-phonon coupling in kagome superconductor KV_3Sb_5 , arXiv:2107.02688 (2021).
- [30] A. Bolens and N. Nagaosa, Topological states on the breathing kagome lattice, *Phys. Rev. B* **99**, 165141 (2019).
- [31] M. L. Kiesel and R. Thomale, Sublattice interference in the kagome Hubbard model, *Phys. Rev. B* **86**, 121105R (2012).
- [32] W. S. Wang, Z. Z. Li, Y. Y. Xiang, and Q.-H. Wang, Competing electronic orders on kagome lattices at van Hove filling, *Phys. Rev. B* **87**, 115135 (2013).
- [33] M. L. Kiesel, C. Platt, and R. Thomale, Unconventional Fermi Surface Instabilities in the Kagome Hubbard Model, *Phys. Rev. Lett.* **110**, 126405 (2013).
- [34] T. C. Hsu, J. B. Marston, and I. Affleck, Two observable features of the staggered-flux phase at nonzero doping, *Phys. Rev. B* **43**, 2866 (1991).
- [35] S. Chakravarty, R. B. Laughlin, D. K. Morr, and C. Nayak, Hidden order in the cuprates, *Phys. Rev. B* **63**, 094503 (2001).
- [36] C. M. Varma, Theory of the pseudogap state of the cuprates, *Phys. Rev. B* **73**, 155113 (2006).
- [37] X. Fang, K. Jiang, Z. Wang, and J. Hu, Chiral flux phase in the kagome superconductor AV_3Sb_5 , *Science Bulletin* **66**, 1384 (2021).
- [38] M. M. Denner, R. Thomale, and T. Neupert, Analysis of charge order in the kagome metal AV_3Sb_5 ($A=K, Rb, Cs$), arXiv:2103.14045, (2021).
- [39] T. Park, M. Ye, and L. Balents, Electronic instabilities of kagome metals: saddle points and Landau theory, *Phys. Rev. B* **104**, 035142 (2021).
- [40] Y.-P. Lin and R. M. Nandkishore, Complex charge density waves at Van Hove singularity on hexagonal lattices: Haldane-model phase diagram and potential realization in kagome metals AV_3Sb_5 ($A=K, Rb, Cs$), *Phys. Rev. B* **104**, 045122 (2021).
- [41] B. R. Ortiz, et al., Fermi surface mapping and the nature of charge density wave order in the kagome superconductor CsV_3Sb_5 , arXiv:2104.07230 (2021).
- [42] Y. Fu, et al., Quantum transport evidence of topological band structures of kagome superconductor CsV_3Sb_5 , arXiv:2104.08193 (2021).
- [43] W. L. McMillan, Landau theory of charge-density waves in transition-metal dichalcogenides, *Phys. Rev. B* **12**, 1187 (1975).
- [44] D. F. Agterberg, M. Geracie, and H. Tsunetsugu, Conventional and charge-six superfluids from melting hexagonal Fulde-Ferrell-Larkin-Ovchinnikov phases in two dimensions, *Phys. Rev. B* **84**, 014513 (2011).
- [45] D. Agterberg and H. Tsunetsugu, Dislocations and vortices in pair-density-wave superconductors, *Nat. Phys.* **4**, 639 (2008).
- [46] Z. Dai, Y.-H. Zhang, T. Senthil, and P. A. Lee, Pair-density waves, charge-density waves, and vortices in high- T_c cuprates, *Phys. Rev. B* **97**, 174511 (2018).
- [47] D. F. Agterberg et al., The Physics of Pair-Density Waves: Cuprate Superconductors and Beyond, *Annu. Rev. Condens. Matter Phys.* **11**, 231 (2020).
- [48] E. Berg, E. Fradkin, and S. A. Kivelson, Charge-4e superconductivity from pair-density-wave order in certain high-temperature superconductors, *Nat. Phys.* **5**, 830 (2009).
- [49] A. P. Schnyder, S. Ryu, A. Furusaki, and A. W. Ludwig, Classification of topological insulators and superconductors in three spatial dimensions, *Phys. Rev. B* **78**, 195125 (2008).
- [50] Z. Wang, G. Kotliar, X.-F. Wang, Flux-density wave and superconducting instability of the staggered-flux phase, *Phys. Rev. B* **42**, 8690(R) (1990).
- [51] Vivek Aji, Arkady Shekhter, and C. M. Varma, Theory of the coupling of quantum-critical fluctuations to fermions and d -wave superconductivity in cuprates, *Phys. Rev. B* **81**, 064515 (2010).
- [52] P. A. Lee, Amperean pairing and the pseudogap phase of cuprate superconductors, *Phys. Rev. X* **4**, 031017 (2014).